Variable inertia effects of an engine including piston friction and a crank or gudgeon pin offset

A L Guzzomi*, **D C Hesterman,** and **B J Stone**
School of Mechanical Engineering, The University of Western Australia, Perth, Western Australia, Australia

The manuscript was received on 27 March 2007 and was accepted after revision for publication on 13 November 2007.

DOI: 10.1243/09544070JAUTO590

Abstract: In order to obtain greater accuracy in simulation, more sophisticated models are often required. When it comes to the torsional vibration of reciprocating mechanisms the effect of inertia variation is very important. It has been shown that the inclusion of this variation increases model accuracy for both single-cylinder and multi-cylinder engine torsional vibration predictions. Recent work by the present authors has revealed that piston-to-cylinder friction may modify an engine's 'apparent' inertia function. Kinematic analysis also shows that the piston side force and the dynamic piston-to-cylinder friction are interdependent. This has implications for engine vibration modelling. Most modern engines employ a gudgeon pin offset, and there is a growing interest in pursuing large crank offsets; hence, the effect of these on inertia variation is also of interest. This paper presents the derivation of the inertia function for a single engine mechanism, including both piston-to-cylinder friction and crank or gudgeon pin offset, and investigates the effect of each through predictions. The effect of crank offset on the variable inertia function is also verified by experiment.

Keywords: variable inertia, crank offset, gudgeon pin offset, piston friction, torsional vibration

1 INTRODUCTION

The automotive industry is an extremely competitive market where success demands innovation conceived through simulation prior to production. A greater desire for physical understanding requires increased prediction accuracy, which can be obtained by more detailed modelling of component interactions. Considerations such as difficulty in model derivation, computation time, and desired accuracy are all factors in determining the level of sophistication warranted. Previously, noise, vibration, and harshness [**1**–**3**] were attributed as the deciding factors in customer quality perception that influenced the possible success or failure in the market place. However, with the ever-heightened awareness of human environmental impact or footprint, there is a substantial push to lessen emissions and to increase efficiency. This in turn has seen a substantial research effort towards understanding friction behaviour and the development of engine models incorporating detailed friction models used for simulation for fuel economy, vibration, and noise purposes [**4**–**8**].

It is well established [**2**, **8**–**16**] that a single reciprocating engine has a mass moment of inertia which changes with crank angle. This is due to the piston and connecting-rod centre-of-mass (COM) positions changing their location with respect to the crankshaft axis. The resulting inertia function is periodic and can be approximated as a constant inertia with a superimposed second-order cosine. In most published models the cyclical nature of the inertia is ignored and an average inertia is used to calculate the average torsional natural frequencies and critical speeds. However, it can be shown that the frequency content (amplitude and phase) of the inertia function introduces non-linear coupling between the engine speed and the average torsional natural frequencies [**17**]. This coupling produces secondary resonance peaks, or side bands, on the

**Corresponding author: School of Mechanical Engineering, The University of Western Australia, 35 Stirling Hwy Crawley, Perth, Western Australia, 6009, Australia. email: aguzzomi@mech.uwa.edu.au and anolrew.guzzomi@mail.ing.unibo.it*

average natural frequencies. Excitation at a sideband frequency can feed energy into the average natural frequency and produce a phenomenon called 'secondary resonance' [**11**]. In multi-cylinder engines the crankshaft configuration is designed in part to minimize inertia variation; however, crankshaft flexibility and other design constraints prevent its elimination. In large low-speed configurations typical of diesel engines used in marine applications, generator sets, and large earth-moving equipment, secondary resonance can still be a problem [**17**]. Current design methods for these types of powertrain try to account for the extra mechanical stress produced by secondary resonance (see, for example reference [**18**]), although this area of vibration is still not fully understood. Additionally, Rahnejat [**19**] has identified that the future trend in internal combustion engine development will be towards smaller lightweight engines with fewer cylinders; this in turn will lead to larger variations in the imbalance forces and torques. A review of literature pertaining to secondary resonance has been given by Hesterman and Stone [**9**]. The inertia of any engine will affect its performance and, for real-time monitoring and control of reciprocating engines, it is important to assess whether the variation in inertia should be included in the engine model. Some have said that the inclusion of variable inertia is necessary when modelling reciprocating engines to increase prediction accuracy for crank angular displacement, velocity, and acceleration [**20**]. This is particularly true when the crankshaft configuration does not eliminate the inertia variation, e.g. in a four-cylinder engine, or when the crankshaft is flexible. Also, as mentioned above, the inclusion of the variable inertia function allows non-linear frequency coupling in the engine to be evaluated.

Hesterman and Stone [**13**] presented equations for the inertia function and rate of change in inertia for a single reciprocating mechanism in the absence of gudgeon pin or crank offset and friction. Drew *et al.* [**21**] then used this model to investigate the natural frequency function of a small single-cylinder engine. Measurements on an engine were also performed, using discrete-position oscillation tests. A servomotor was used to oscillate the engine. The results showed that the natural frequency of the engine varied with the crank angle, with good agreement between predicted and measured values. There were, however, small differences noted when the piston was located near midstroke. Guzzomi *et al.* [**4**] studied the same motored engine and found that piston-to-cylinder friction influences the moment experienced by the engine block. Large discrepancies between measurements and predictions may occur when the piston-to-cylinder friction is ignored, especially at low crank rotational speed. Their work also revealed that the piston side force is a function of piston-to-cylinder friction, the two being interrelated by the geometry of the mechanism. This was unexpected as friction is traditionally assumed to be independent of the normal contact force. However, a kinetic analysis of the reciprocating mechanism shows that the piston side force is a function of the vertical loading on the piston (the combustion force, etc). In this context, piston-to-cylinder friction also represents a vertical loading on the piston and thus affects the side force as well. It may also be shown that the piston side force appears in the equations used to develop the engine's inertia function. This means that piston-to-cylinder friction affects the 'apparent' inertia of the engine. This in turn will affect the natural frequency function. Guzzomi *et al.* [**22**] revisited the work presented in reference [**23**] and demonstrated that the differences between prediction and measurement around midstroke are most probably due to piston-to-cylinder friction.

As noted, recent research has very much focused on increasing efficiency. According to Zweiri *et al.* [**20**], recent regulations have imposed stringent emission and fuel economy standards that cannot be addressed by a steady state analysis of the engine. Mechanical losses due to friction account for between 4 per cent and 15 per cent of the total energy consumed in modern internal combustion engines [**24**]. Approximately half of engine losses are attributed to the piston rings and half from the piston skirt and only a small part of the friction is due to the connecting pin [**24**]. From these studies, piston friction has been identified as a significant contributor to system energy loss; the general consensus is that the conjunction between the ring-pack and the cylinder bore is the main contributor [**25**]. In order to increase the efficiency the reduction of piston frictional losses is highly desired. The piston ring and skirt reactions have also been identified as contributors to noise characteristics [**26**]. There is a substantial research effort aimed towards understanding friction behaviour and the development of engine models incorporating detailed friction models. According to Wong *et al.* [**24**], the behaviour of the skirt-to-cylinder contact is a function of connecting-rod angle, gas loading, film thickness, and velocity. The models have been used to investigate fuel economy [**7**], vibration, and noise

issues. Friction losses, especially in the piston assembly, are important when modelling transient behaviour, because they strongly affect the economy, performance, and durability of the reciprocating internal combustion engine [**20**].

As the need for more accurate real-time models has arisen, attempts have been made to include friction (piston-to-cylinder friction in particular) and variable inertia. Typically, piston-to-cylinder friction is included as an equivalent friction torque or is investigated mostly under hydrodynamic conditions in the absence of inertial dynamics [**19**, **23**, **27**]. If variable inertia effects are included, then these too are usually represented as an externally applied torque instead of an intrinsic behaviour of the engine. In such cases, an equivalent second-order reciprocating torque is used to model the effect of a variable inertia. However, by assigning equivalent friction or inertia torques, their interdependence is lost. Also, non-linear coupling effects between engine speed and the average torsional natural frequencies, which can result in potentially troublesome running speeds, remain unknown.

Stringent vehicle emission standards have required industry and researchers to improve engine acoustic performance and fuel efficiency. To address noise and wear problems, nearly all reciprocating engines now employ offset gudgeon (wrist) pins [**25**]. An offset helps the mechanism move through the top-dead-centre (TDC) position in the presence of combustion. In 2001, Zweiri *et al.* [**8**] published equations for the crankshaft torque experienced by a single-cylinder engine with inertia variation, gudgeon pin offset, and combustion effects included. These equations have been used in a number of subsequent papers [**23**, **28**, **29**]. There are, however, a number of errors in their kinematic and kinetic analyses of the mechanism. There is an inconsistency with the crank angle definition and some terms have incorrect sign conventions. The variable inertia of the piston and conrod also appear to be included twice, once in the inertia function and then also as a reciprocating torque. Despite these errors, Zweiri *et al.* showed good correlation between predictions and measurements taken on a combustion-powered engine. This would indicate that the errors do not affect the model predictions greatly. Results using the published equations in reference [**8**] are presented in this paper for comparison purposes. While the gudgeon pin offset is controlled by the size and design constraints placed on the piston, larger changes in mechanism geometry can be achieved by offsetting the crank. One advantage of large offsets is that they offer the potential to increase engine torque, by allowing the crank and connecting rod to be more perpendicular to each other when combustion occurs. This has led to a growing body of literature on crank offsetting and a number of patents in the area [**30**–**32**]. Large crank offsets have also been investigated as a means of reducing friction to increase fuel economy [**20**]. The effect of such offsets on inertia variation does not appear to have been investigated.

The main focus of this paper is the development of a model for a reciprocating engine, which includes variable inertia effects, gudgeon or crank pin offset, and piston-to-cylinder friction. The model is derived using a dynamic analysis of a single reciprocating mechanism. Friction is included in the initial free-body diagrams and the inertia function is determined from the equations. This method ensures that any non-linear behaviour is retained in the model and it also avoids the need to apply external torques to represent inertia and friction effects after the model has been derived. The effect of offset and some of the effects of piston-to-cylinder friction on the resulting inertia function are then investigated and discussed. Experimental verification of the effect of crank offset on the variable inertia function of a single cylinder engine is also included. Experimental verification of other aspects of the model have been presented in previously published papers [**4**, **21**, **22**].

2 MODEL DERIVATION

The kinematic and kinetic analyses presented in this section build on the equations originally presented by Hesterman and Stone [**13**]. Their equations are given in Appendix 2 for easy reference. Inclusion of a crank or gudgeon pin offset changes only one of their equations; however, to include piston friction the equations must be substantially reworked. A full list of the assumptions made by Hesterman and Stone in deriving their model can be found in reference [**13**]. The same assumptions are made in this analysis, with the exception that piston friction is non-zero. The critical assumptions are as follows.

1. The crank, connecting rod, and piston act as rigid bodies.
2. Bearing stiffness and friction are not included.
3. All forces on the piston act through the gudgeon pin and the piston remains collinear to the cylinder bore. The gudgeon pin is taken as the COM position of the piston.

Assumption 3 simplifies the analysis and is considered reasonable for a piston that has a centrally located gudgeon pin and is symmetrical in the plane of the mechanism about its longitudinal axis. Including a crank offset does not affect the symmetry of such a piston and thus is not expected to increase the likelihood of piston tilt. The assumption becomes more questionable when the gudgeon pin is offset, because the piston geometry must become asymmetric. This introduces extra uncertainty about the line of action of each force on the piston. However, in most engines the gudgeon pin offset is very small and the assumption of no piston tilt may still be acceptable. Hence, piston tilt is not expected to have a significant effect on the variable inertia function of an engine.

2.1 Kinematic analysis

With reference to Fig. 1, it can be shown schematically that a crank offset is analogous to a gudgeon pin offset when considering the geometry of the mechanism. This means that the kinematic analyses will be the same for both cases. The piston displacement z is measured from the crankshaft bearing at O to the gudgeon pin at B. Thus,

$$z = r\cos\theta - l\cos\phi \tag{1}$$

where

$$l\sin\phi = \delta + r\sin\theta \tag{2}$$

Equation (2) is the same as equation (22), except for the inclusion of the offset term δ. This offset is constant for a particular engine and vanishes when equation (2) is differentiated. Thus, the resulting expressions for $\dot{\phi}$ and $\ddot{\phi}$ are the same as those given in equations (23) and (24) respectively. The piston velocity $\dot{z}$ is also required in order to determine the direction of the piston-to-cylinder frictional force. Differentiating equation (1) gives

$$\dot{z} = r\dot{\theta}(\cos\theta\tan\phi - \sin\theta) \tag{3}$$

The general expressions for the COM accelerations of the piston, connecting rod, and crank are not affected by the offset and are given in equations (25) to (30).

2.2 Kinetic analysis

Figure 2 shows the free-body diagrams for the piston, connecting rod, and crank. The piston diagram on the left was that used by Hesterman and Stone [**13**] and that on the right is the model used in this paper. The diagrams and kinetic equations for the connecting rod and crank are the same for both models. The equations derived in reference [**13**] are used in the analysis below and are given in Appendix 2.

In developing the piston free-body diagram to include friction, it is assumed that piston-to-cylinder friction is dominated by two interactions: ring friction F_r produced by the static ring tension applying a distributed force against the cylinder wall, and dynamic friction μS produced by the piston side force S as the piston translates up or down the cylinder. Ignoring the gap in the piston rings, and any variation in the friction value around the piston, it is reasonable to group the distributed ring pack friction force as shown in Fig. 2. Under the assumption that the piston remains collinear to the cylinder bore (no piston tilt), any moment produced by dynamic friction about the gudgeon pin must be

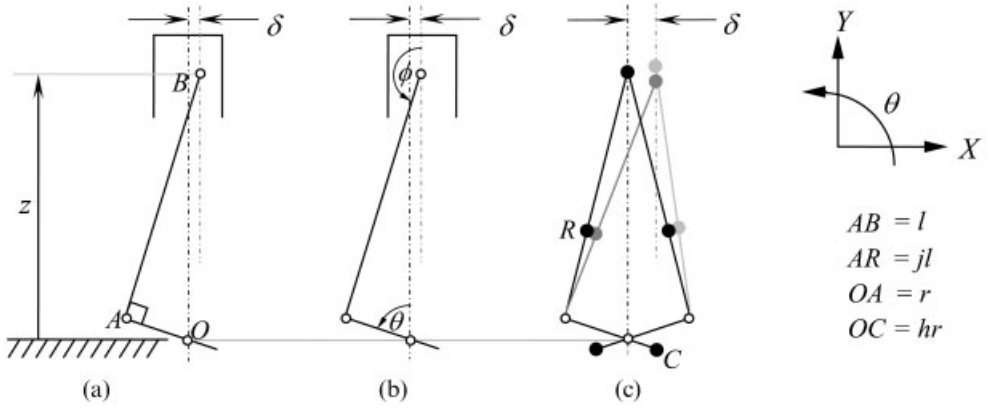

Fig. 1 Schematic representation of engine mechanism with (a) a gudgeon offset, (b) a crank offset, and (c) the COM locations for an offset mechanism

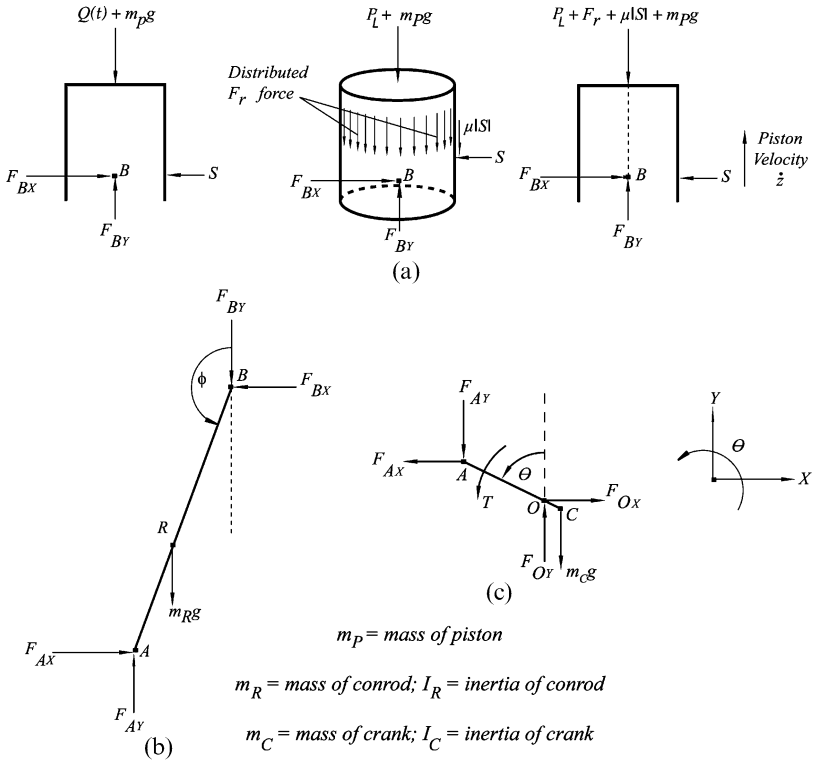

Fig. 2 Freebody diagrams of (a) the piston (b) the connecting rod, and (c) the crank

balanced by the piston side force. Thus, the side force will move up and down the piston to ensure the net moment is zero. It can be shown that this case is equivalent to the side force S acting through the gudgeon pin and both F_r and μS acting through the piston crown [**4**]. It is noted that, as the piston diameter and piston-to-cylinder clearance increase, the assumption of no piston tilt becomes less valid. However, for the engine considered in this paper the assumption is reasonable. A general pressure loading force on the piston crown is also included and represented by P_L. Note that S, μ, F_r, and P_L may be functions of time and/or crank position. If it is assumed that all forces on the piston act through the gudgeon pin, then a comparison between the left and right free-body diagrams of the piston in Fig. 2 reveals that piston-to-cylinder friction can be introduced into the model developed by Hesterman and Stone [**13**] using the substitution

$$Q(t) = P_L + F_r \pm \mu S \tag{4}$$

The sign of the μS term depends on the direction of piston travel and the direction of S. F_r also depends on the direction of piston travel, but this is taken into account in the mathematical function used to describe this term. Combining equation (4) with equation (32), the equation for piston motion in the Y direction then becomes

$$F_{BY} - m_P g - P_L - F_r \mp \mu S = m_P a_{PY} \tag{5}$$

It is important to note that the X and Y equations for the piston, defined by equations (31) and (5), are now coupled with the piston side force S appearing in both. All further manipulation of the equations must take this into account.

A new expression for the piston side force can be obtained by combining equations (31) and (33) to (35) with equation (5), and then substituting for the COM accelerations using equations (25) to (28). After some rearranging,

$$\begin{aligned} S = \Bigg\{ & -r\ddot{\theta}\left[\frac{I_R \cos\theta}{(l\cos\phi)^2} + m_P \tan\phi(\cos\theta\tan\phi - \sin\theta)\right. \\ & \left. + jm_R\left(\frac{j\cos\theta}{\cos^2\phi} - \sin\theta\tan\phi - \cos\theta\right)\right] \\ & - r\dot{\theta}^2\left[\frac{I_R}{(l\cos\phi)^2}\left(\frac{r\cos^2\theta\tan\phi}{l\cos\phi} - \sin\theta\right)\right. \\ & + m_P\tan\phi\left(\frac{r\cos^2\theta}{l\cos^3\phi} - \sin\theta\tan\phi - \cos\theta\right) \\ & \left. + jm_R\left(\frac{jr\cos^2\theta\tan\phi}{l\cos^3\phi} - \cos\theta\tan\phi + \sin\theta - \frac{j\sin\theta}{\cos^2\phi}\right)\right] \\ & - g\tan\phi(m_P + jm_R) - F_r\tan\phi - P_L\tan\phi\Bigg\}\frac{1}{D(\mu)} \end{aligned} \tag{6}$$

where

$$D(\mu)=\begin{cases} 1+\mu\tan\phi, & \begin{cases}\dot{z}\geqslant 0, & S\geqslant 0\\ \dot{z}<0, & S<0\end{cases}\\ 1-\mu\tan\phi, & \begin{cases}\dot{z}\geqslant 0, & S<0\\ \dot{z}<0, & S\geqslant 0\end{cases}\end{cases} \tag{7}$$

Comparing the above expressions with equation (39), which is the model for S derived in reference [**13**], it is evident that friction adds significant complexity to the piston side force. In fact, equations (6) and (7) reveal that the side force and piston-to-cylinder friction are interdependent. This behaviour has been verified and studied in some detail in reference [**4**]. A new expression for the applied crankshaft torque T can also be found using equations (5) to (7). Rearranging equation (38) and substituting for the bearing forces gives

$$\begin{aligned} T=&I_{\mathrm{C}}\ddot{\theta}+m_{\mathrm{C}}a_{\mathrm{C}X}hr\cos\theta-m_{\mathrm{R}}a_{\mathrm{R}X}r\cos\theta\\ &+m_{\mathrm{C}}a_{\mathrm{C}Y}hr\sin\theta-m_{\mathrm{R}}a_{\mathrm{R}Y}r\sin\theta\\ &-m_{\mathrm{P}}a_{\mathrm{P}Y}r\sin\theta+m_{\mathrm{C}}hgr\sin\theta\\ &-m_{\mathrm{R}}gr\sin\theta-m_{\mathrm{P}}gr\sin\theta-P_{\mathrm{L}}r\sin\theta\\ &-F_{\mathrm{r}}r\sin\theta-Sr(\cos\theta\pm\mu\sin\theta) \end{aligned} \tag{8}$$

Then, replacing the COM accelerations with equations (25) to (30) and grouping terms gives

$$\begin{aligned} T=&\ddot{\theta}\{I_{\mathrm{C}}+m_{\mathrm{C}}h^2r^2-m_{\mathrm{P}}r^2(\cos\theta\tan\phi-\sin\theta)\sin\theta\\ &+m_{\mathrm{R}}r^2[(1-j)\cos^2\theta-(j\cos\theta\tan\phi-\sin\theta)\sin\theta]\}\\ &-\dot{\theta}^2\left[m_{\mathrm{P}}r^2\left(\frac{r\cos^2\theta}{l\cos^3\phi}-\cos\theta-\sin\theta\tan\phi\right)\sin\theta\right.\\ &+m_{\mathrm{R}}r^2(1-j)\cos\theta\sin\theta\\ &\left.+m_{\mathrm{R}}r^2\left(\frac{jr\cos^2\theta}{l\cos^3\phi}-\cos\theta-j\sin\theta\tan\phi\right)\sin\theta\right]\\ &+gr(m_{\mathrm{C}}h\sin\theta-m_{\mathrm{R}}\sin\theta-m_{\mathrm{P}}\sin\theta)-P_{\mathrm{L}}r\sin\theta\\ &-F_{\mathrm{r}}r\sin\theta-Sr(\cos\theta\pm\mu\sin\theta) \end{aligned} \tag{9}$$

Finally, substituting for S from equations (6) and (7)

$$T=\ddot{\theta}I_{\mathrm{f}}(\theta)+\frac{1}{2}\dot{\theta}^2I'_{\mathrm{f}}(\theta)+g_{\mathrm{f}}(\theta)+P_{\mathrm{f}}(t,\theta) \tag{10}$$

where $I_{\mathrm{f}}(\theta)$ is the 'apparent' inertia function given by

$$\begin{aligned} I_{\mathrm{f}}(\theta)=&I_{\mathrm{C}}+m_{\mathrm{C}}h^2r^2+I_{\mathrm{R}}E(\mu)\left(\frac{r\cos\theta}{l\cos\phi}\right)^2\\ &+m_{\mathrm{P}}r^2(\cos\theta\tan\phi-\sin\theta)\\ &[E(\mu)\cos\theta\tan\phi-\sin\theta]\\ &+m_{\mathrm{R}}r^2\{(1-j)[1-jE(\mu)]\cos^2\theta\\ &+(j\cos\theta\tan\phi-\sin\theta)[jE(\mu)\cos\theta\tan\phi-\sin\theta]\} \end{aligned} \tag{11}$$

$I'_{\mathrm{f}}(\theta)$ is the 'apparent' rate of change in inertia with respect to crank angle θ given by

$$\begin{aligned} I'_{\mathrm{f}}(\theta)=&2I_{\mathrm{R}}E(\mu)\left(\frac{r\cos\theta}{l\cos\phi}\right)^2\left(\frac{r\cos\theta}{l\cos\phi}\tan\phi-\tan\theta\right)\\ &+2m_{\mathrm{P}}r^2[E(\mu)\cos\theta\tan\phi-\sin\theta]\\ &\left(\frac{r\cos^2\theta}{l\cos^3\phi}-\cos\theta-\sin\theta\tan\phi\right)\\ &-2m_{\mathrm{R}}r^2(1-j)^2\sin\theta\cos\theta\\ &+2m_{\mathrm{R}}r^2[jE(\mu)\cos\theta\tan\phi-\sin\theta]\\ &\left(\frac{jr\cos^2\theta}{l\cos^3\phi}-\cos\theta-j\sin\theta\tan\phi\right) \end{aligned} \tag{12}$$

$g_{\mathrm{f}}(\theta)$ is the modified gravity torque for a vertically mounted mechanism given by

$$\begin{aligned} g_{\mathrm{f}}(\theta)=&gr\{m_{\mathrm{P}}[E(\mu)\cos\theta\tan\phi-\sin\theta]\\ &+m_{\mathrm{R}}[jE(\mu)\cos\theta\tan\phi-\sin\theta]+m_{\mathrm{C}}h\sin\theta\} \end{aligned} \tag{13}$$

$P_{\mathrm{f}}(t,\ \theta)$ is the torque due to ring friction and pressure loading on the piston given by

$$P_{\mathrm{f}}(t,\theta)=(P_{\mathrm{L}}+F_{\mathrm{r}})r[E(\mu)\cos\theta\tan\phi-\sin\theta] \tag{14}$$

and

$$E(\mu)=\begin{cases}\dfrac{1+\mu\tan\theta}{1+\mu\tan\phi}, & \begin{cases}\dot{z}\geqslant 0, & S\geqslant 0\\ \dot{z}<0, & S<0\end{cases}\\ \dfrac{1-\mu\tan\theta}{1-\mu\tan\phi}, & \begin{cases}\dot{z}\geqslant 0, & S<0\\ \dot{z}<0, & S\geqslant 0\end{cases}\end{cases} \tag{15}$$

Equations (10) to (14) may be compared directly with equations (41) to (45) respectively. In doing so it is evident how the piston friction modifies each expression. With reference to equations (42) and (43), it may be shown that $I'(\theta)$ is the derivative of $I(\theta)$ with respect to the crank angle

θ [**13**]. This is not the case when friction is included. The expressions for $I_f(\theta)$ and $I'_f(\theta)$, given above in equations (11) and (12), both contain the term $E(\mu)$. $E(\mu)$ is a function of crank angle and $dE(\mu)/d\theta$ is non-zero for most values of θ. However, $I'_f(\theta)$ does not contain $dE(\mu)/d\theta$. Comparing equation (12) with equation (43), it can be seen that $I'_f(\theta)$ has the same form as $I'(\theta)$, except for the inclusion of $E(\mu)$ in some terms. When μ is set to zero, $E(\mu) = 1$, and the above equations simplify to those given in Appendix 2.

3 MODEL PREDICTIONS

A theoretical investigation of the effects of crank offset and piston friction is presented in this section. In order to separate the influence of each, a frictionless mechanism with crank offset is considered first. The piston friction is then explored in a mechanism with no offset. Although the main focus of this paper is on the inertia function and how this changes with offset and friction, other terms in the torque equation (31) are also investigated. The data used in the engine model is taken from reference [**32**], with $r \approx 25$ mm and $l \approx 100$ mm. Unless otherwise specified, all results in this section are for counter-clockwise (CCW) crank rotation with reference to Fig. 1.

3.1 Crank or gudgeon pin offset

The equations given in Appendix 2 may be used when friction in the mechanism is ignored. To include crank or gudgeon pin offset, equation (2) replaces equation (22). The predicted inertia functions for a range of offset values are given in Fig. 3. Zero on the abscissa corresponds to crank TDC. Figure 3(a) shows the inertia function for the case of zero offset, using equation (42) and the corresponding expression from the work of Zweiri *et al.* [**8**]. The inertia function with zero offset is expected to be symmetrical about bottom dead centre (BDC), because of the symmetrical path followed by the mechanism. It is clear from Fig. 3(a) that the equations published in reference [**8**] predict an asymmetrical function and thus are fundamentally incorrect. The magnitudes are, however, consistent with the model presented in this paper and the equation predicts part of the inertia function correctly. Figures 3(b) and (c) show the effect of a non-zero offset. For the engine used in these predictions, a realistic gudgeon pin offset of 1.0 mm has a negligible impact on the inertia. Even a shift of 10 mm introduces a relatively small change. Although a 10 mm offset in gudgeon pin position is unrealistic for the engine considered, it would be possible to achieve this by offsetting the crank. Figure 3(c) shows the inertia function for a positive offset, with reference to Fig. 1, and Fig. 3(d) shows the result for a negative offset of the same magnitude. The COM positions of a reciprocating mechanism, with zero and positive offset, are shown in Fig. 1(c) at two crank locations. It can be seen that the mechanism geometry is different when an offset is included for each crank angle. For CCW rotation the connecting rod and piston positions on the mechanism with a positive offset are more advanced than the mechanism with zero offset. This behaviour will produce an inertia function that leads the zero-offset case. A negative offset will produce the opposite effect. This lead–lag behaviour is evident in Figs 3(c) and (d). To explain this further, the relative contributions of the piston, connecting rod, and crank to the inertia function need to be evaluated. To do this, equation (42) may be rewritten in component form as

$$I(\theta) = I_C(\theta) + I_{R1}(\theta) + I_{R2}(\theta) + I_P(\theta) \tag{16}$$

where

$$I_C(\theta) = I_C + m_C h^2 r^2 = \text{constant} \tag{17}$$

$$I_{R1}(\theta) = I_R \left(\frac{r \cos\theta}{l \cos\phi} \right)^2 \tag{18}$$

$$\begin{aligned} I_{R2}(\theta) &= m_R r^2 \left[(1-j)^2 \cos^2\theta + (j \cos\theta \tan\phi - \sin\theta)^2 \right] \\ &= j m_R r^2 (\cos\theta \tan\phi - \sin\theta)^2 \\ &\quad + (1-j) m_R r^2 \left(1 - \frac{j \cos^2\theta}{\cos^2\phi} \right) \end{aligned} \tag{19}$$

$$I_P(\theta) = m_P r^2 (\cos\theta \tan\phi - \sin\theta)^2 \tag{20}$$

Figure 4 shows the connecting-rod and piston inertia functions over one crank revolution. Two cases are considered: zero offset, and a positive offset of 10 mm. The contribution to system inertia from the connecting rod's mass moment of inertia $I_{R1}(\theta)$ is illustrated in Fig. 4(a). The connecting rod experiences significant rotation when the connecting rod and crank are collinear and little rotation

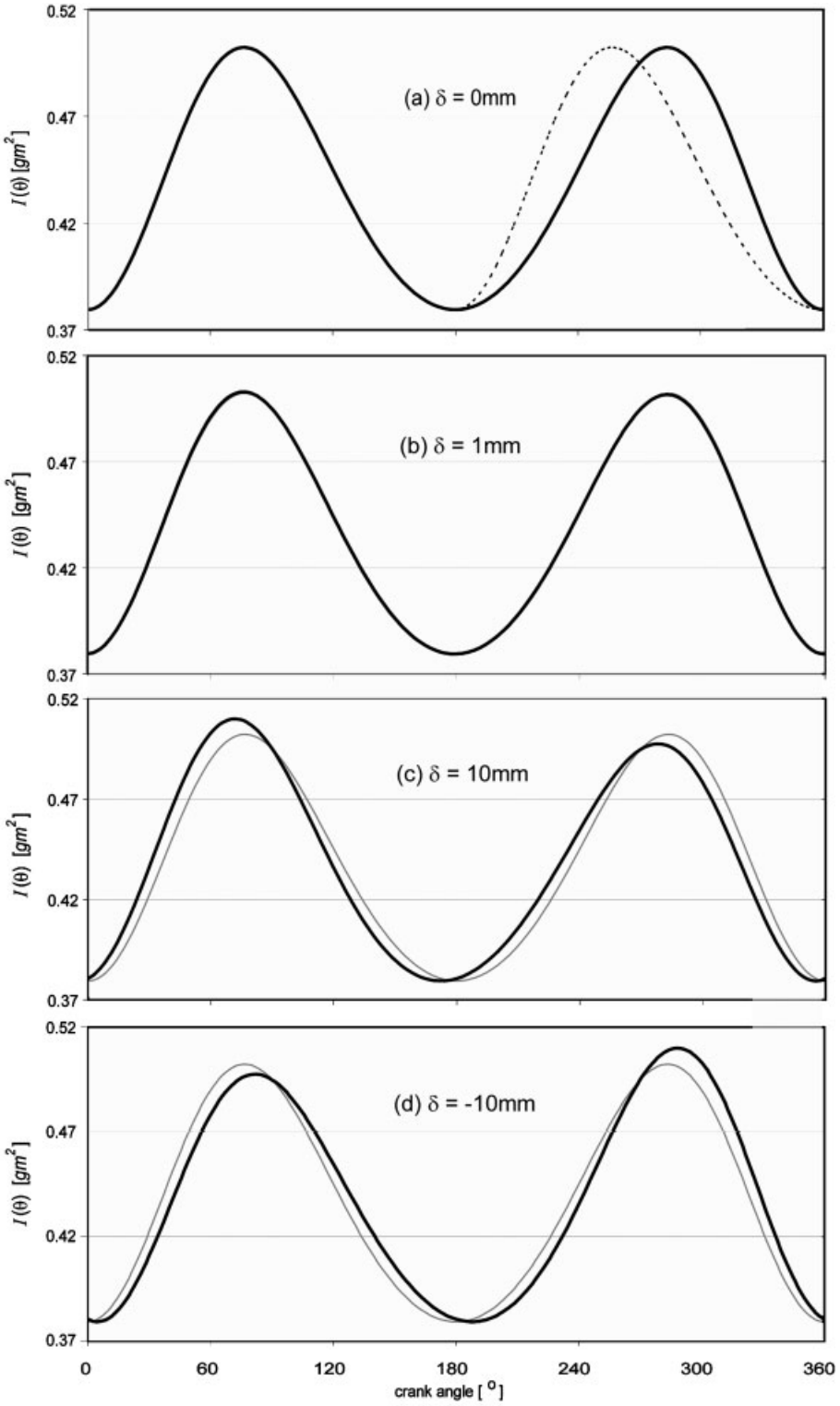

Fig. 3 Predicted inertia function in the absence of friction for various offset values: —, $\delta = 0$; —, $\delta \neq 0$; ---, $\delta = 0$ using equations from reference [**8**], shown in (a) only. All plots are for CCW crank rotation

when travelling through midstroke. As a consequence, $I_{R1}(\theta)$ is a maximum at or near the crank dead-centre (DC) positions, and a minimum around midstroke. Equation (18) shows this term becomes zero when $\theta = 90^{\circ}$. The contributions to system inertia from the piston mass ($I_P(\theta)$), and the

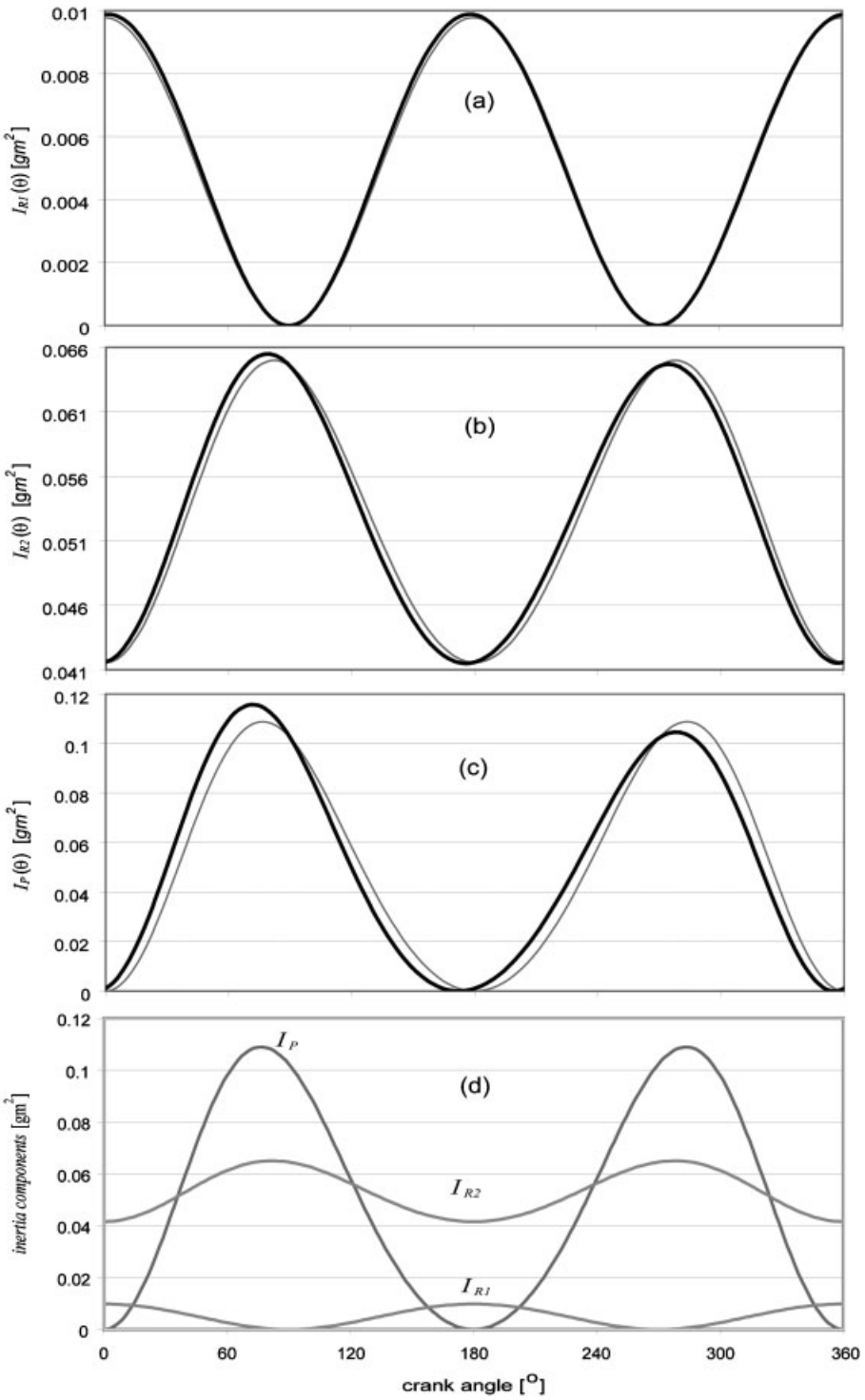

Fig. 4 Piston and connecting-rod inertia components: —, $\delta = 0$; —, $\delta = 10$ mm. All plots are for CCW crank rotation with no friction

connecting-rod mass, ($I_{R2}(\theta)$) are shown in Figs 4(b) and (c) respectively. They follow an opposite trend to $I_{R1}(\theta)$. The reciprocating mass (piston and part of the connecting rod) experiences very little motion around the DC positions and, thus, does not contribute much mass loading or inertia to the system at these locations. Around midstroke, however, the piston experiences significant motion for a small change in crank angle and the reciprocating inertia increases. The maximum piston inertia occurs when the crank and connecting rod are essentially perpendicular to each other. Equation

(19) identifies how much of the connecting-rod mass reciprocates with the piston and how much rotates with the crank. The ratio is controlled by the parameter j. When $j = 0$, the COM of the connecting rod coincides with the main bearing at A and all the connecting-rod mass rotates with the crank. Equation (19) reduces to the inertia about O of a lumped mass at A. When $j = 1$, the COM of the connecting rod is located at the gudgeon pin B and all the connecting-rod mass reciprocates with the piston. In this case, equation (19) has the same form as equation (20). Figure 4(d) allows the relative contribution of each inertia term to be evaluated. It can be seen that the maximum amplitude of $I_{R1}(\theta)$ is a tenth of that of the effective piston inertia for the engine considered in this paper. $I_{R1}(\theta)$ is ignored in simplified models of engines. The differences observed between the inertia function of a mechanism with zero offset and one with a non-zero offset are due to the relationship between θ and ϕ (see equation (2)). The largest change occurs in the effective piston inertia $I_P(\theta)$ shown in Fig. 4(c). The asymmetry in the piston and connecting-rod inertia functions is introduced by the cos θ tan ϕ – sin θ expression in equations (19) and (20). Figure 5 shows the effect of offset on this expression.

The rotation direction of the crankshaft will modify the effect of an offset, and this is illustrated in Fig. 6. The results in Fig. 6(a) are for a mechanism rotating CCW with a positive offset of 10 mm. Those in Fig. 6(b) are for clockwise (CW) rotation with a negative offset of 10 mm. As expected, the prediction in Fig. 6(a) is simply a reflection of that shown in Fig. 6(b). Inertia predictions using the equations published in reference [**8**] are also given. The prediction for the case in Fig. 6(a) is a reasonable match for most of the cycle and agrees with the shape published in reference [**8**]. Errors in the equations are exacerbated for the case in Fig. 6(b).

In summary, typical values of gudgeon pin offset have a negligible effect on the inertia function of an engine. In such cases the offset can be ignored. For large crank offsets, however, the effect is more pronounced with observable changes in the magnitude and phase of the inertia function. Similar results are observed in the functions for $I'(\theta)$ and $g(\theta)$. These modified functions will influence engine behaviour and thus their inclusion in engine models will improve real-time prediction accuracy. These changes may also hold significant implications for the non-linear frequency coupling associated with variable-inertia systems. It is noted that the effects of any offset will increase with an increase in piston and connecting-rod mass.

3.2 Piston friction

A theoretical investigation of how piston friction affects the inertia function is presented in this section. Equations (10) to (15) are used for

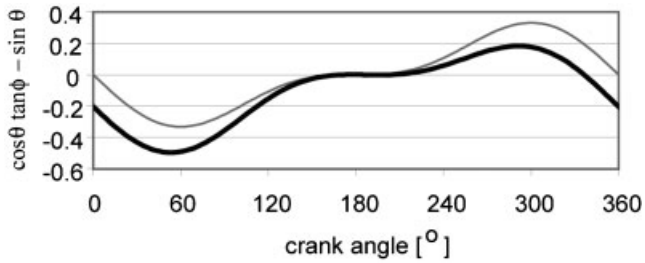

Fig. 5 Effect of an offset of $\delta = 10$ mm on cos θ tan ϕ − sin θ

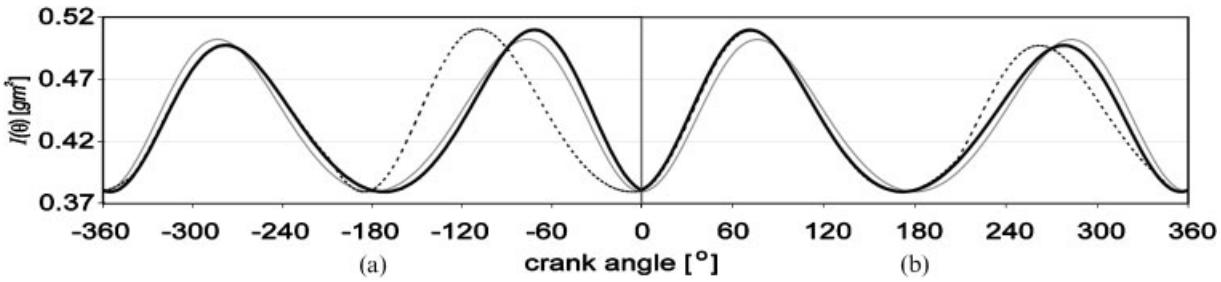

Fig. 6 The effect of offset and crankshaft rotation direction with no friction for (a) $\delta = -10$ mm and CW rotation and (b) $\delta = 10$ mm and CCW rotation: —, $\delta = 0$; —, $\delta \neq 0$; ---, $\delta \neq 0$ using equations from reference [**8**]

predictions. Only the zero-offset case is studied. Typical friction values measured on a small motored single-cylinder engine are used. Details of how these values were obtained can be found in reference [**4**]. A magnitude of 40 N is used for the ring friction F_r, and the dynamic coefficient μ of friction is taken as 0.3. Although this friction coefficient value is large for periods when high lubricant entrainment can be expected (midstroke), higher values may be experienced when the piston is near TDC or BDC (piston velocity very low). In practice, the coefficient changes throughout the engine cycle [**4–6**, **33–37**]. However, it is not the purpose of this paper to perform a detailed friction analysis, but rather to show the mathematical relationship which gives rise to the interaction. The effects of dynamic friction increase as μ increases, and a value of 0.3 allows its influence to be clearly observed. The results presented are for a constant engine speed of 44 rad/s (276 r/min). At this speed, ring friction dominates system behaviour. At high engine speeds the dynamic friction term μS becomes significant and the behaviour of the system changes [**4**]. Thus, the results shown in Fig. 7 are valid for low speeds.

Figure 7 shows the effect of piston friction on the different torque components of equation (10). The 'apparent' inertia function, predicted from equation (11), is given in Fig. 7(a). Friction does not change the inertia value at the DC positions when $\delta = 0$, because $E(\mu)$ is equal to one at these positions. This will not be the case when an offset is introduced; a small phase shift is expected. Friction does have a noticeable effect around midstroke, with the 'apparent' inertia increasing. As expected, the 'apparent' average inertia of the mechanism increases and more energy is required to drive the system when friction is included. It is noted that the value used for μ in the predictions is larger than would be expected for standard midstroke lubrication and loading conditions. Therefore the relative change in inertia will usually be less than that shown in Fig. 7(a). The effect of piston friction on the 'apparent' rate of change in inertia is illustrated in Fig. 7(b). The result is predicted using equation (12). Comparing the graphs in Fig. 7(a) with those in Fig. 7(b), it is evident that $I'_f(\theta)$ follows the expected shape of the true derivative of $I_f(\theta)$. The gravity and loading torque terms are shown in Figs 7(c) and (d), respectively. Equations (13) and (14) are used for the predictions. The inclusion of piston friction reduces the gravity torque during the first half of the cycle, when gravity assists motion and increases the torque during the second half, when gravity opposes motion. In the absence of pressure forces on the

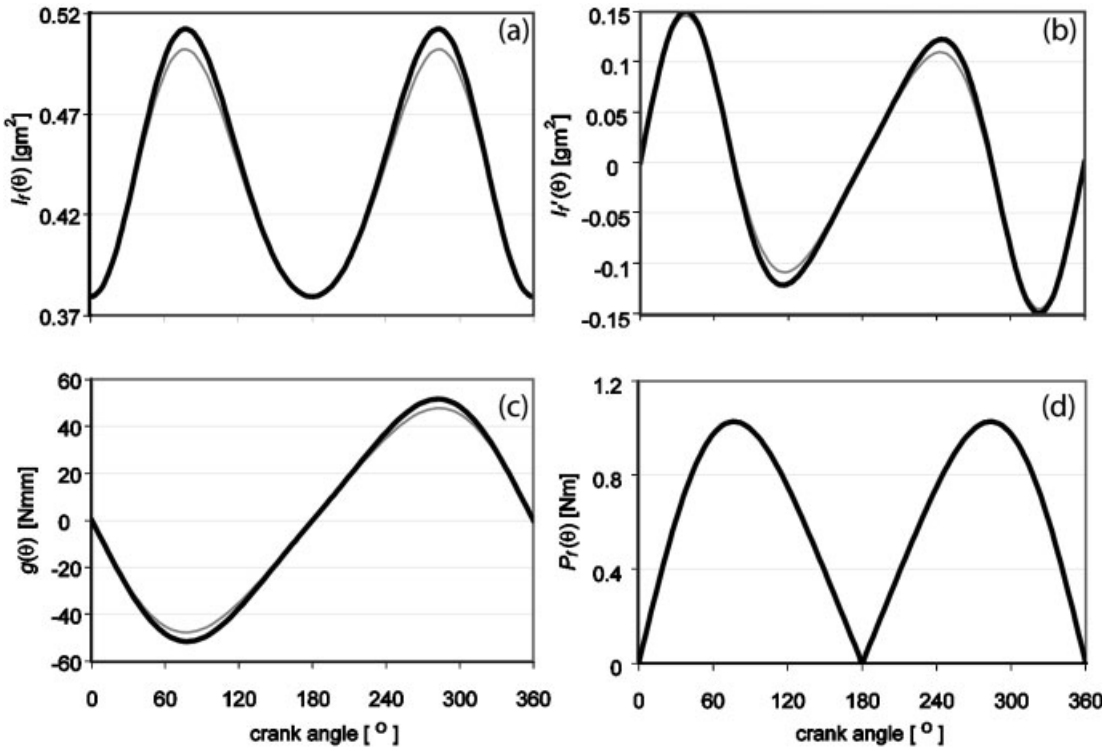

Fig. 7 Crankshaft torque components: —, $|F_r| = \mu = 0$; — $|F_r| = 40$ N, $\mu = 0.3$. All plots are for CCW crank rotation at 44 rad/s with $\delta = 0$

piston, only F_r appears in equation (14) and this term goes to zero when friction is ignored. As expected, it can be seen that a large torque resists motion when ring friction is included. A more detailed discussion of this torque, including how speed and friction magnitudes affect its behaviour, has been given in reference [**4**].

4 EXPERIMENTAL VERIFICATION

This section presents the experimental work conducted to verify the effect of offset on an engine's inertia function. Guzzomi *et al.* [**22**] have already reported an experimental investigation of piston-to-cylinder friction and its effect on engine inertia. Results from that study confirm model predictions and show that piston-to-cylinder friction does increase the 'apparent' inertia during midstroke travel.

The experimental set-up used to investigate gudgeon pin offset was similar to that used in reference [**23**] and is shown schematically in Fig. 8. The rig consisted of a 120 cm^3 Villiers single-cylinder engine with the flywheel, cylinder head, camshaft, and timing gear removed. Most of the physical parameters pertaining to the engine can be found in reference [**23**]. The variable inertia effect was enhanced by increasing the piston mass by 42 per cent. To permit offset in the plane of the mechanism, the engine block was cut so that the base, housing the crankshaft main bearings, could be translated with respect to the cylinder bore. This meant that both the base and the bore had to be supported separately. A 10 mm crank offset was used in the tests. This was the maximum offset possible before the lower part of the cylinder bore interfered with the motion of the connecting rod. For smaller values, it was difficult to observe differences in the inertia function when comparing it against the zero-offset case. The effect of friction was minimized by removing all rings from the piston and applying oil to the bore prior to each test. The simplified engine mechanism was torsionally excited using a servo motor via a strain-gauged shaft. Non-rotating tests at discrete crank positions were conducted. A large protractor (degree wheel) was attached to the crankshaft to allow the angle of the crank to be determined to within $\pm 1^\circ$. The inbuilt swept sine and autoresolution facilities of a signal analyser were used to excite the engine mechanism at each position. A TAP^{TM} (angular) accelerometer was located at the free end of the crankshaft to measure the angular response.

The rig was modelled as a two-degree-of-freedom lumped-mass system as shown in Fig. 8. The motor was represented as an inertia attached to a rotating abutment via a spring and viscous damper [**23**]. The shafting between the strain gauge and the engine inertia was modelled as a simple equivalent spring of stiffness k. It was assumed that friction and viscous damping in the engine mechanism were negligible; however, frequency response measurements showed small amounts of damping were present.

At each crank angle, there was expected to be a frequency for which the motor would have negligible motion and the response of the engine mechanism would be a maximum. When this occurs, the engine mechanism is behaving as a detuner for the motor and shafting. This was found to be the case. The response can then be approximated by

$$\left|\frac{\Theta}{T_m}\right|_{max} = \frac{1}{k - I(\theta)\omega_n^2} \tag{21}$$

For each crank position θ, the frequency corresponding to the maximum response of the engine subsystem was determined using the TAP^{TM} accelerometer and the strain-gauged shaft torque. A swept sine of constant amplitude was used for the

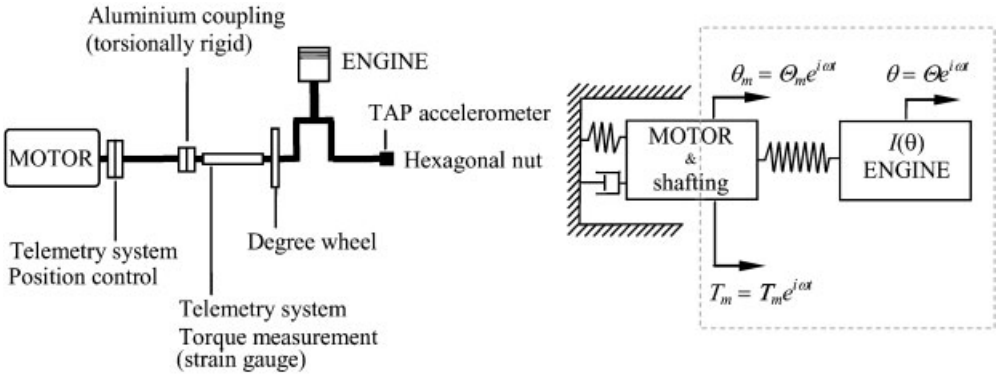

Fig. 8 Schematic diagram of the test rig and an equivalent lumped mass model

excitation. The acceleration and torque measurements were then used in equation (21) to estimate the engine inertia. The complex geometry of the shafting made it difficult to calculate an equivalent stiffness analytically; hence, a constant value for k was also estimated from the measurements. This was found to be in reasonable agreement with a value calculated using the geometry. Inertia values were determined for a range of discrete crank angles using this method and the results are shown in Fig. 9. Model predictions using equation (2) and the equations in Appendix 2 are also shown for the cases of zero offset and an offset of 10 mm. It can be seen that the prediction with offset is in very good agreement with the 'measured' inertia results, both displaying the same phase lags and amplitude modulations. As mentioned earlier, small amounts of damping were observed in the measured frequency response functions. However, this was not enough to change the estimated inertia values significantly. Discrepancies between the 'measured' and predicted inertia functions are most probably due to errors in the system parameters used in the model, and the simplistic model used for the inertia estimates.

5 CONCLUSION

This paper has presented a mathematical model for a single reciprocating mechanism that includes a variable mass moment of inertia, a crank or gudgeon pin offset, and piston-to-cylinder friction. The model extends the work reported in reference [**13**]. It does not approximate friction or inertia as externally applied torques but includes them in the model derivation. The model was used to investigate the effects of offset and piston friction on the inertia function of a single mechanism, and experimental work was reported that verifies model predictions for a small single-cylinder engine. The main findings are summarized below.

The inclusion of a crank or gudgeon pin offset in the model was straightforward, with only one equation changing from those published in reference [**13**]. More significant changes to the model were required to include piston-to-cylinder friction. The kinetic analysis revealed that the piston side force S is a function of any vertical loading on the piston; hence, S is a function of piston-to-cylinder friction. This means that the side force and the frictional force are interdependent. The relationship between these two terms is dictated by the geometry of the reciprocating mechanism. As a result, it is insufficient simply to 'add' an equivalent friction torque into the mechanism's torque equation when including the effects of piston friction. The torque equation must be determined from the original component equations of motion. When this is carried out, the coefficient of dynamic friction appears in a number of the torque terms, including the 'apparent' inertia function of the mechanism and the 'apparent' rate of change in inertia.

The model was then used to investigate the effects of offset on the inertia function of a single reciprocating mechanism, with no friction present. The inertia predictions were consistent with expectations, and a previously published model [**8**] was shown to contain errors. Results from the model presented here indicate that, for typical values, the gudgeon pin offset does not have a significant affect on the inertia function. However, for the larger values used in crank offsets, the inclusion of the offset in the engine model improves the prediction accuracy. Large crank offsets introduce a noticeable phase change and amplitude asymmetry in the

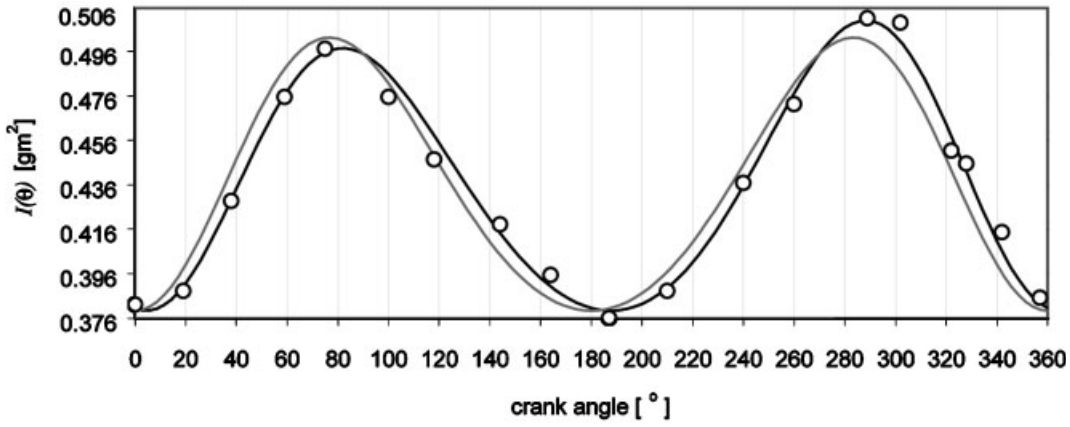

Fig. 9 Measured and predicted inertia functions: —, prediction with $\delta = 0$; — prediction with $\delta = 10$ mm; O, measured with $\delta = 10$ mm

inertia function. Experimental work on a small single-cylinder engine confirmed model predictions.

Previous work by the present authors has shown that piston-to-cylinder friction must be included in engine models, especially those used for real-time applications. At low speeds, dynamic friction plays a very small part and piston-to-cylinder friction can be modelled as ring friction only. At high speeds, the effect of dynamic friction becomes significant and should also be included. In this paper, the effect of piston friction on the 'apparent' inertia function was investigated. Results for the case of zero offset showed that the inclusion of friction has negligible effect at TDC and BDC, but it increases the 'apparent' inertia around midstroke. This has been verified experimentally in reference [**22**]. One outcome of this behaviour is that the 'apparent' average inertia of the engine increases; however, it should be noted that a relatively large value for the dynamic coefficient of friction was used in the predictions and only a very small change in average inertia was determined.

The study presented in this paper has been restricted to the effects of offset and piston-to-cylinder friction on an engine's variable inertia function. However, the model can be used to study the general behaviour of both single-cylinder and multi-cylinder engines. Equation (10) allows variable inertia, offset, and piston-to-cylinder friction to be included in the expression for the crankshaft torque. More recently the present authors have used the model to investigate the non-linear behaviour of reciprocating engines. Preliminary results show that changes in the phase and the amplitude of the frequency content of the inertia function will affect frequency coupling in an engine. The relationship between dynamic friction and the inertia function has also been shown to influence this behaviour. It is the intention of the present authors to present these findings in a future paper.

ACKNOWLEDGEMENTS

The authors would like to acknowledge the financial assistance to Dr A. L. Guzzomi from the William Lambden Owen Scholarship fund and the Robert Maude Gledden Scholarship fund during his PhD candidature. The completion of this paper was performed while Dr Guzzomi was a University of Western Australia Whitfeld Fellow conducting research at the University of Bologna.

REFERENCES

1 **Schumacher, T., Biermann, J.-W., Jansz, N., Willey, J.,** and **Kupper, K.** Load change reactions of passenger cars: method of investigation and improvement. *Proc. Instn Mech. Engrs, Part K: J. Multi-body Dynamics*, 2003, **217**(4), 283–291.

2 **Boysal, A.** and **Rahnejat, H.** Torsional vibration analysis of a multi-body single cylinder internal combustion engine model. *Appl. Mathl Modelling*, 1997, **21**(8), 481–493.

3 **Farshidianfar, A., Ebrahimi, M., Rahnejat, H., Menday, M.,** and **Moavenian, M.** Optimization of the high-frequency torsional vibration of vehicle driveline systems using genetic algorithms. *Proc. Instn Mech. Engrs, Part K: J. Multi-body Dynamics*, 2002, **216**, 249–262.

4 **Guzzomi, A. L., Hesterman, D. C.,** and **Stone, B. J.** The effect of piston friction on engine block dynamics. *Proc. IMechE, Part K: J. Multi-body Dynamics*, 2006, **221**(2), 277–289.

5 **Mufti, R. A., Priest, M.,** and **Chittenden, R. J.** Experimental and theoretical study of instantaneous piston assembly friction in a gasoline engine. In Proceedings of the 2004 ASME/STLE International Joint Tribology Conference, Long Beach, California, USA, October 2004, pp. 907–921.

6 **Mistry, K., Bhatt, D. V.,** and **Sheth, N. R.** Theoretical modeling and simulation of piston ring assembly of an IC engine. In Proceedings of the 2004 ASME/STLE International Joint Tribology Conference, Long Beach, California, USA, October 2004.

7 **Richardson, D. E.** Review of power cylinder friction for diesel engines. *Trans. ASME, J. Engng Gas Turbines Power*, 2000, **122**(4), 506–519.

8 **Zweiri, Y. H., Whidborne, J. F.,** and **Seneviratne, L. D.** Detailed analytical model of a single-cylinder diesel engine in the crank angle domain. *Proc. Instn Mech. Engrs, Part D: J. Automobile Engineering*, 2001, **215**(11), 1197–1216.

9 **Hesterman, D. C.** and **Stone, B. J.** Secondary inertia effects in the torsional vibration of reciprocating engines – a literature review. *Proc. Instn Mech. Engrs, Part C: J. Mechanical Engineering Science*, 1995, **209**(1), 11–15.

10 **Hesterman, D. C.** and **Stone, B. J.** A comparison of secondary inertia effects in a range of reciprocating engines. In Proceedings of the International Mechanical Engineering Congress, Canberra, Australia, 1994, pp. 1–6.

11 **Hesterman, D. C., Drew, S. J.,** and **Stone, B. J.** Vibration of engines resulting from torsional vibration of crankshafts. In Proceedings of the Conference on *Vibrations in rotating machinery*, 1996, vol. 1, pp. 713–723 (Mechanical Engineering Publications Limited, London).

12 **Rajendran, S.** and **Narasimhan, M. V.** Effect of inertia variation due to reciprocating parts and connecting rod on coupled vibration of crankshaft. *Trans. ASME, J. Engng Gas Turbines Power*, 1997, **119**(1), 257–264.

13 **Hesterman, D. C.** and **Stone, B. J.** A systems approach to the torsional vibration of multi-cylinder reciprocating engines and pumps. *Proc.*

Instn Mech. Engrs, Part C: J. Mechanical Engineering Science, 1994, **208**(6), 395–408.
14 **Hesterman, D. C.** *Torsional vibrations in reciprocating pumps and engines*. PhD Thesis, Department of Mechanical Engineering, University of Western Australia, Perth, Western Australia, 1992, p. 178.
15 **Guzzomi, A. L., Hesterman, D. C.,** and **Stone, B. J.** Torsional vibration of engines. In Proceedings of the 12th International Conference on Sound and Vibration, Lisbon, Portugal, July 2005, pp. 1–8.
16 **Brusa, E., Delprete, C.,** and **Genta, G.** Torsional vibration of crankshafts: effects of non-constant moments of inertia. *J. Sound Vibr.*, 1997, **205**(2), 135–150.
17 **Pasricha, M. S.** Effect of damping on parametrically excited torsional vibrations of reciprocating engines including gas forces. *J. Ship Res.*, 2006, **50**(2), 147–157.
18 **Schiffer, W.** Advanced methods for static and dynamic shafting calculations. *J. Nav. Architecture Shipbldg Industry (Brodogradnja)*, 2007, **58**(2), 158–164.
19 **Rahnejat, H.** *Multi-body dynamics*, 1998, p. 355 (Professional Engineering Publishing Limited, Bury St Edmunds).
20 **Zweiri, Y. H., Whidborne, J. F.,** and **Seneviratne, L. D.** Dynamic simulation of a single-cylinder diesel engine including dynamometer modelling and friction. *Proc. Instn Mech. Engrs, Part D: J. Automobile Engineering*, 1999, **213**(4), 391–402.
21 **Drew, S. J., Hesterman, D. C.,** and **Stone, B. J.** Torsional excitation of variable inertia effects in a reciprocating engine. *Mech. Systems Signal Processing*, 1999, **13**(1), 125–144.
22 **Guzzomi, A. L., Hesterman, D. C.,** and **Stone, B. J.** The effect of piston friction on the torsional natural frequency of a reciprocating engine. *Mechl Systems Signal Processing*, 2007, **21**(7), 2833–2837.
23 **Zweiri, Y. H., Whidborne, J. F.,** and **Seneviratne, L. D.** A comparison of dynamic models of various complexity for diesel engines. *Mathl Computer modelling Dynamical Systems*, 2002, **8**(3), 273–289.
24 **Wong, V., Tian, T., Moughon, L., Takata, R.,** and **Jocsak, J.** Low-engine-friction technology for advanced natural-gas reciprocating engines. Annual Technical Progress Report, Massachesetts Institute of Technology, Cambridge, Massachesetts, 30 June 2006.
25 **Balakrishnan, S.** and **Rahnejat, H.** Isothermal transient analysis of piston skirt-to-cylinder wall contacts under combined axial, lateral and tilting motion. *J. Physics D: Appl. Physics*, 2005, **38**(5), 787–799.
26 **Betz, G., Gabele, H.,** and **Assmus, H.-O.** Friction power and noise behaviour of the piston assembly. In Proceedings of the Second International Conference on Combustion Engines – Reduction of Friction and Wear, London, September 1989, pp. 35–58.
27 **Ma, Z.-D.** and **Perkins, N. C.** An efficient multibody dynamics model for internal combustion engine systems. *Multibody System Dynamics*, 2003, **10**(4), 363–391.
28 **Zweiri, Y. H.** Diesel engine indicated torque estimation based on artificial neural networks. *Int. J. Intell. Technol.*, 2006, **1**(3), 233–239.
29 **Zweiri, Y. H.** and **Seneviratne, L. D.** Diesel engine indicated and load torque estimation using a non-linear observer. *Proc. IMechE, Part D: J. Automobile Engineering*, 2006, **220**(6), 775–785.
30 **Garvin, E. A.** Offset crankshaft mechanism for an internal combustion engine. US Pat. 5816201, 1998.
31 **Lee, C. L.** Offset crankshaft engine. US Pat. 6058901, 2000.
32 **Nyström, R.** Device for converting a linear movement into a rotary movement. US Pat. 6851401, 2005.
33 **Priest, M., Dowson, D.,** and **Taylor, C. M.** Theoretical modelling of cavitation in piston ring lubrication. *Proc. Instn Mech. Engrs, Part C: J. Mechanical Engineering Science*, 2000, **214**, 435–447.
34 **Xu, H., Bryant, M. D., Matthews, R. D., Kiehne, T. M.,** and **Steenwyk, B. D.** Friction predictions for piston ring–cylinder liner lubrication. In Proceedings of the 2004 Fall Technical Conference of the ASME Internal Combustion Engine Division, Long Beach, California, USA, 2004, pp. 773–784 (American Society of Mechanical Engineers, New York).
35 **Thring, R. H.** Piston skirt friction in internal combustion engines. ASME Paper S7-1CE-20, 1987.
36 **Smith, E. H., Clark, C. A.,** and **Sherrington, I.** The measurement of piston assembly friction in a motored engine. IMechE Conference on Universal and Poly Research on IC Engines, 1991, pp. 185–190.
37 **Sherrington, I.** and **Smith, E. H.** The measurement of piston/piston-ring friction by the 'floating –liner' method. In Proceedings of the IMechE Seminar on *Engine research and development*, 1988, pp. 1–11 (Mechanical Engineering Publications Limited, London).

APPENDIX 1

Notation

a	acceleration vector
A	big-end (connecting-rod) bearing position
B	gudgeon pin position
C	centre-of-mass position of the crank
COM	centre of mass
$D(\mu)$, $E(\mu)$	convenient groupings of terms
F_A	big-end (connection-rod) reaction
F_B	gudgeon pin reaction
F_r	frictional force produced by piston ring static tension
g	acceleration due to gravity

$g(\theta)$	gravity torque about O without piston-to-cylinder friction
$g_f(\theta)$	gravity torque about O with piston-to-cylinder friction included
h	ratio of the length OC to the length OA ($0<h<1$)
$I(\theta)$	inertia function of the reciprocating mechanism without friction
$I'(\theta)$	rate of change in the inertia function with respect to the crank angle
I_C	inertia of crank about its centre of mass
$I_C(\theta)$	constant inertia of the crank
$I_f(\theta)$	'apparent' inertia function of the reciprocating mechanism with friction
$I'_f(\theta)$	'apparent' rate of change in the inertia function with friction
$I_p(\theta)$	piston inertia contribution due to its mass
I_R	inertia of the connecting rod about its centre of mass
$I_{R1}(\theta)$	connection-rod inertia contribution due to its inertia
$I_{R2}(\theta)$	connecting-rod inertia contribution due to its mass
j	ratio of the length AR to the length AB ($0<j<1$)
k	equivalent torsional stiffness
l	length of the connecting rod = AB
m_C	mass of the crank
m_P	mass of the piston
m_R	mass of the connecting rod
O	main crank bearing
P_L	generic pressure loading on the piston along the cylinder axis
$Q(t)$	piston loading along the cylinder axis
$Q(t,\theta)$	torque about O due to $Q(t)$
r	crank throw = OA
R	centre-of-mass position of the connecting rod
S	piston side force
T	crank torque
z	piston displacement = OB
δ	gudgeon offset from the crank bearing parallel to the cylinder bore
θ	angular displacement of the crank (relative to the block)
μ	kinetic coefficient of friction
ϕ	angular displacement of the connecting rod (relative to the cylinder bore)
ω_n	natural frequency

APPENDIX 2

Hesterman and Stone [**13**] presented a dynamic analysis of a vertically mounted single reciprocating mechanism without crank or gudgeon pin offset. They assumed that the mechanism was frictionless and that there was a generic piston loading force $Q(t)$ acting on the crown of the piston. The main equations describing their model are summarized below.

Kinematic analysis

With reference to Fig. 1 with offset $\delta = 0$,

$$l \sin \phi = r \sin \theta \tag{22}$$

Differentiating gives

$$\dot{\phi} = \frac{r\dot{\theta} \cos \theta}{l \cos \phi} \tag{23}$$

$$\ddot{\phi} = \dot{\theta}^2 \left[\left(\frac{r \cos \theta}{l \cos \phi} \right)^2 \tan \phi - \frac{r \sin \theta}{l \cos \phi} \right] + \ddot{\theta} \frac{r \cos \theta}{l \cos \phi} \tag{24}$$

Relative velocity and acceleration analyses were performed in reference [**13**] to determine the COM accelerations of the piston, connecting rod, and crank. Equations (23) and (24) were then used in these expressions to replace $\dot{\phi}$ and $\ddot{\phi}$ respectively. Differentiation of the geometry relationships yields the same results. For the piston,

$$a_{PX} = 0 \tag{25}$$

$$a_{PY} = \dot{\theta}^2 \left(\frac{(r \cos \theta)^2}{l \cos^3 \phi} - r \cos \theta - r \sin \theta \tan \phi \right) + \ddot{\theta}(r \cos \theta \tan \phi - r \sin \theta) \tag{26}$$

For the connecting rod,

$$a_{RX} = \dot{\theta}^2 (1-j) r \sin \theta - \ddot{\theta}(1-j) r \cos \theta \tag{27}$$

$$a_{RY} = \dot{\theta}^2 \left[j \frac{(r \cos \theta)^2}{l \cos^3 \phi} - r \cos \theta - jr \sin \theta \tan \phi \right] + \ddot{\theta}(jr \cos \theta \tan \phi - r \sin \theta) \tag{28}$$

For the crank,

$$a_{CX} = -\dot{\theta}^2 hr \sin\theta + \ddot{\theta} hr \cos\theta \tag{29}$$

$$a_{CY} = \dot{\theta}^2 hr \cos\theta + \ddot{\theta} hr \sin\theta \tag{30}$$

Kinetic analysis

The free-body diagrams used in reference [**13**] are shown in Fig. 2, with the appropriate piston diagram on the left of Fig. 2(a). All forces on the piston are assumed to act through the gudgeon pin. The dynamic equations for the piston, connecting rod, and crank are then as follows. For the piston,

$$\begin{aligned} &\sum F_X = m_{\mathrm{p}} a_{\mathrm{p}X} = 0 \\ &F_{\mathrm{B}X} - S = 0 \\ &F_{\mathrm{B}X} = S \end{aligned} \tag{31}$$

$$F_{\mathrm{B}Y} - m_{\mathrm{p}} g - Q(t) = m_{\mathrm{p}} a_{\mathrm{p}Y} \tag{32}$$

For the connecting rod,

$$\begin{aligned} &\sum F_X = m_{\mathrm{R}} a_{\mathrm{R}X} \\ &F_{\mathrm{A}X} - F_{\mathrm{B}X} = m_{\mathrm{R}} a_{\mathrm{R}X} \end{aligned} \tag{33}$$

$$\begin{aligned} &\sum F_Y = m_{\mathrm{R}} a_{\mathrm{R}Y} \\ &F_{\mathrm{A}Y} - F_{\mathrm{B}Y} - m_{\mathrm{R}} g = m_{\mathrm{R}} a_{\mathrm{R}Y} \end{aligned} \tag{34}$$

$$\begin{aligned} &\sum M_{\mathrm{R}} = I_{\mathrm{R}} \ddot{\phi}_{\mathrm{R}} \\ &-F_{\mathrm{B}X}(1-j) l \cos\phi - F_{\mathrm{B}Y}(1-j) l \sin\phi \\ &-F_{\mathrm{A}X} jl \cos\phi - F_{\mathrm{A}Y} jl \sin\phi = I_{\mathrm{R}} \ddot{\phi}_{\mathrm{R}} \end{aligned} \tag{35}$$

For the crank,

$$\begin{aligned} &\sum F_X = m_{\mathrm{C}} a_{\mathrm{C}X} \\ &F_{\mathrm{O}X} - F_{\mathrm{A}X} = m_{\mathrm{C}} a_{\mathrm{C}X} \end{aligned} \tag{36}$$

$$\begin{aligned} &\sum F_Y = m_{\mathrm{C}} a_{\mathrm{C}Y} \\ &F_{\mathrm{O}Y} - F_{\mathrm{A}Y} - m_{\mathrm{C}} g = m_{\mathrm{C}} a_{\mathrm{C}Y} \end{aligned} \tag{37}$$

$$\begin{aligned} &\sum M_{\mathrm{C}} = I_{\mathrm{C}} \ddot{\theta}_{\mathrm{C}} \\ &T + F_{\mathrm{A}X}(1+h) r \cos\theta + F_{\mathrm{A}Y}(1+h) r \sin\theta \\ &-F_{\mathrm{O}X} hr \cos\theta - F_{\mathrm{O}Y} hr \sin\theta = I_{\mathrm{C}} \ddot{\theta}_{\mathrm{C}} \end{aligned} \tag{38}$$

An expression for the piston side force S can be obtained by combining equations (31) to (34) with equation (35), and then substituting for the COM accelerations using equations (25) to (28), according to

$$\begin{aligned} S = &-r\ddot{\theta}\left[\frac{I_{\mathrm{R}} \cos\theta}{(l\cos\phi)^2} + m_{\mathrm{P}} \tan\phi(\cos\theta\tan\phi - \sin\theta)\right. \\ &\left. + jm_{\mathrm{R}}\left(\frac{j\cos\theta}{\cos^2\phi} - \sin\theta\tan\phi - \cos\theta\right)\right] \\ &-r\dot{\theta}^2\left[\frac{I_{\mathrm{R}}}{(l\cos\phi)^2}\left(\frac{r\cos^2\theta\tan\phi}{l\cos\phi} - \sin\theta\right)\right. \\ &+ m_{\mathrm{P}}\tan\phi\left(\frac{r\cos^2\theta}{l\cos^3\phi} - \sin\theta\tan\phi - \cos\theta\right) \\ &\left. + jm_{\mathrm{R}}\left(\frac{jr\cos^2\theta\tan\phi}{l\cos^3\phi} - \cos\theta\tan\phi + \sin\theta - \frac{j\sin\theta}{\cos^2\phi}\right)\right] \\ &- g\tan\phi(m_{\mathrm{P}} + jm_{\mathrm{R}}) - Q(t)\tan\phi \end{aligned} \tag{39}$$

An expression for the crankshaft torque can be obtained by rearranging equation (38) and substituting for the bearing forces to give

$$\begin{aligned} T = &I_{\mathrm{C}}\ddot{\theta} + m_{\mathrm{C}} a_{\mathrm{C}X} hr\cos\theta - m_{\mathrm{R}} a_{\mathrm{R}X} r\cos\theta \\ &+ m_{\mathrm{C}} a_{\mathrm{C}Y} hr\sin\theta - m_{\mathrm{R}} a_{\mathrm{R}Y} r\sin\theta - m_{\mathrm{P}} a_{\mathrm{P}Y} r\sin\theta \\ &+ m_{\mathrm{C}} hgr\sin\theta - m_{\mathrm{R}} gr\sin\theta - m_{\mathrm{P}} gr\sin\theta \\ &- Q(t) r\sin\theta - Sr\cos\theta \end{aligned} \tag{40}$$

Substituting for the COM accelerations and grouping like terms result in

$$T = \ddot{\theta} I(\theta) + \frac{1}{2}\dot{\theta}^2 I'(\theta) + g(\theta) + Q(t, \theta) \tag{41}$$

where $I(\theta)$ is the mechanism's inertia function given by

$$\begin{aligned} I(\theta) = &I_{\mathrm{C}} + m_{\mathrm{C}} h^2 r^2 + I_{\mathrm{R}}\left(\frac{r\cos\theta}{l\cos\phi}\right)^2 \\ &+ m_{\mathrm{P}} r^2(\cos\theta\tan\phi - \sin\theta)^2 \\ &+ m_{\mathrm{R}} r^2\left[(1-j)^2\cos^2\theta + (j\cos\theta\tan\phi - \sin\theta)^2\right] \end{aligned} \tag{42}$$

$I'(\theta)$ is the rate of change in inertia with respect to the crank angle θ and is given by

$$I'(\theta) = 2I_{\mathrm{R}}\left(\frac{r\cos\theta}{l\cos\phi}\right)^2\left(\frac{r\cos\theta}{l\cos\phi}\tan\phi - \tan\theta\right) + 2m_{\mathrm{P}}r^2(\cos\theta\tan\phi - \sin\theta)\left(\frac{r\cos^2\theta}{l\cos^3\phi} - \cos\theta - \sin\theta\tan\phi\right) - 2m_{\mathrm{R}}r^2(1-j)^2\sin\theta\cos\theta + 2m_{\mathrm{R}}r^2(j\cos\theta\tan\phi - \sin\theta)\left(\frac{jr\cos^2\theta}{l\cos^3\phi} - \cos\theta - j\sin\theta\tan\phi\right) \quad (43)$$

$g(\theta)$ is the gravity torque given by

$$g(\theta) = gr[m_{\mathrm{P}}(\cos\theta\tan\phi - \sin\theta) + m_{\mathrm{R}}(j\cos\theta\tan\phi - \sin\theta) + m_{\mathrm{C}}h\sin\theta] \quad (44)$$

and $Q(t, \theta)$ is the torque produced by the general piston loading term $Q(t)$ acting on the piston crown and is given by

$$Q(t, \theta) = Q(t)r(\cos\theta\tan\phi - \sin\theta) \quad (45)$$